Available online at www.sciencedirect.com
ScienceDirect
International Journal of Heat and Fluid Flow 29 (2008) 94–106
International Journal of HEAT AND FLUID FLOW
www.elsevier.com/locate/ijhff

Experimental investigation of mixed convective flow over a wavy wall

Simon Kuhn, Philipp Rudolf von Rohr *

Institute of Process Engineering, ETH Zurich, 8092 Zurich, Switzerland

Received 18 June 2007; received in revised form 27 August 2007; accepted 9 September 2007
Available online 31 October 2007

Abstract

An experimental study is carried out to address mixed convection from a heated wavy surface. The channel flow between the sinusoidal surface and a flat top wall is investigated by means of a combined digital particle image velocimetry (DPIV) and planar laser-induced fluorescence (PLIF) technique to examine the spatial variation of the streamwise and wall-normal velocity components, and to assess the concentration field of a tracer dye injected into the fluid. We discuss the influence of mixed convection on turbulence quantities and scalar transport properties. Due to the influence of mixed convection we find asymmetric mean velocity profiles and increased momentum transport in the vicinity of the heated surface. The transport of the tracer dye is characterized by enhanced vertical transport due to buoyancy effects and enhanced spanwise transport due to the presence of longitudinal flow structures induced by the mixed convection. We identify two dominant scalar structures with the most influence on vertical transport. The first one is induced by buoyancy effects, the second one by a combination of buoyancy effects and local wall curvature. Thus the transport properties are additionally enhanced compared to mixed convection from a flat plate by the presence of the wavy surface.

Keywords: Particle image velocimetry; Laser-induced fluorescencel; Mixed convection; Wavy wall

1. Introduction

In many transport processes in geophysical and technical flows the transport of a scalar is involved as a combination of free and forced convection. Mixed convective flows are present in technical applications, such as heat transfer devices, and in geophysical flow situations such as transport processes in plant canopies (Banna et al., 2004). These mixed convective flows are often bound by complex wall geometries, e.g. undulations in heat exchangers to enhance transport processes (e.g. Rush et al., 1999; Dellil et al., 2004). This experimental study addresses the mixed convective flow between a flat top wall and a heated wavy bottom wall. Simultaneous measurements of the two-dimensional fluid velocity and the scalar field of a tracer emanating from a point source are facilitated from a combined digital particle image velocimetry (DPIV) and high-resolving planar laser-induced fluorescence (PLIF) technique. Thus the effect of mixed convection on transport processes in a complex flow situation, characterized by separation and reattachment of the flow due to the presence of the wavy wall, is evaluated.

Previous studies of mixed convective flows focused mainly on horizontal parallel plate configurations. Osborne and Incropera investigated laminar, transitional, and turbulent mixed convection heat transfer for a horizontal parallel plate water channel experimentally (Osborne and Incropera, 1985a,b). They found an increase in heat transfer due to buoyancy effects which is less pronounced for higher Reynolds numbers. Maughan and Incropera addressed the regions of heat transfer enhancement for laminar mixed convection for the same flow configuration (Maughan and Incropera, 1989). Their flow visualization results showed that heat transfer enhancement is preceded by the onset of a secondary flow. Yu et al. carried out a numerical and experimental study to investigate this secondary flow in a mixed convective air flow through a horizontal plane channel (Yu et al., 1997a,b). Their results showed that this secondary flow is in the form of

* Corresponding author.
E-mail address: vonrohr@ipe.mavt.ethz.ch (P.Rudolf von Rohr).

0142-727X/$ - see front matter © 2007 Elsevier Inc. All rights reserved.
doi:10.1016/j.ijheatfluidflow.2007.09.002

Nomenclature

a	half-amplitude of the wave profile (m)
B	channel width (m)
g	acceleration due to gravity (m/s^2)
Gr_l	Grashof number, $g\beta\Delta T\, l^3/v^2$
H	full channel height (m)
l	characteristic length scale (m)
$\dot{q}$	heat flux (W/m^2)
Re_l	Reynolds number, $U_B l/v$
T	temperature (K)
u, v, w	components of the instantaneous fluid velocity (m/s)
U_B	bulk velocity (channel flow) (m/s)
x, y, z	Cartesian coordinates (m)
y_w	profile of the wavy bottom wall (m)

Greek symbols

α	amplitude-to-wavelength ratio, $2a/\Lambda$
β	volumetric thermal expansion coefficient (m^3/kg)
Λ	wavelength of the sinusoidal profile at the bottom wall (m)
v	kinematic viscosity (m^2/s)

Abbreviations

CCD	charge coupled device
DPIV	digital particle image velocimetry
FOV	field of view
Nd:YAG	neodymium:yttrium aluminium garnet ($Y_3Al_5O_{12}$) crystal
PLIF	planar laser-induced fluorescence
PVC	poly vinyl chloride
rms	root mean square
$\langle \cdot \rangle$	time average
$(\cdot)'$	fluctuation

Subscript and superscript

B	bulk quantity
H	channel height (used as length scale)
rms	root mean square
w	wall quantity

longitudinal vortex rolls, which changes to transverse rolls when the Reynolds number is lowered (or the Rayleigh number raised). Zhang et al. addressed the flow patterns and heat transfer enhancement of mixed convective airflow in a rectangular channel (Zhang et al., 2002). Depending on the Rayleigh number they found two-, four-, and six-roll modes of the longitudinal flow structures, each mode has an increased effect on heat transfer enhancement. Several other configurations involving plane surfaces have been investigated with regard to scalar transport. Lin and Chen carried out a numerical study to investigate the effect of rotation on these longitudinal vortices in mixed convective flow over a flat plate (Lin and Chen, 2006). They found that for negative rotation the flow is stabilized since the Coriolis force counteracts the buoyancy force, positive rotation destabilizes the flow. Mixed convection from vertical flat surfaces has also been investigated experimentally (e.g. Ayinde et al., 2006) and numerically (e.g Angirasa et al., 1997; Evans et al., 2005), numerical studies also exist for the mixed convection from vertical wavy surfaces (Yao, 1983; Moulic and Yao, 1989; Jang and Yan, 2004). These studies show lower values for the Nusselt number compared to the corresponding flat plate configuration.

To address the influence of the bounding surface on mixed convective flow in the horizontal configuration wavy walls are chosen as a reference flow case which represent the wall complexity in a well-defined manner. As a test case for the influence of hilly terrain on convection in the atmospheric boundary layer Krettenauer and Schumann investigated the influence of wavy surfaces on thermal convection by means of direct numerical simulation (Krettenauer and Schumann, 1989). Several numerical studies addressed convective heat transfer in channel bound by one or two wavy walls (e.g. Dellil et al., 2004; Metwally and Manglik, 2004). In an experimental study Kruse and Rudolf von Rohr (2006) investigated the transport of heat in a turbulent flow over a heated wavy wall. By employing a particle image thermometry technique the velocity and temperature field was measured simultaneously. Quantitative agreement between large-scale thermal and momentum structures was found. However, all of these studies involving horizontal wavy surfaces were in the forced convection regime, fluid motion due to buoyancy effects has been neglected. The present work addresses these buoyancy effects by applying a combined digital particle image velocimetry and laser-induced fluorescence technique to simultaneously measure the velocity field and the concentration field of a scalar in a channel flow with a heated sinusoidal bottom surface, and thus investigates transport processes in complex mixed convective flows.

2. Flow description

We consider the mixed convective flow between a flat top wall and a heated sinusoidal bottom surface. The bottom surface is characterized by the amplitude-to-wavelength ratio of $\alpha = 2a/\Lambda = 0.1$, having a wavelength of $\Lambda = 30$ mm which is equal to the channel height H. The profile of the wavy wall and the used coordinate system is depicted in Fig. 1. The streamwise coordinate direction is denoted by x, the vertical direction by y, and z is the spanwise direction. The corresponding velocity components are denoted as u, v, and w. The profile of the wavy walls can be calculated by

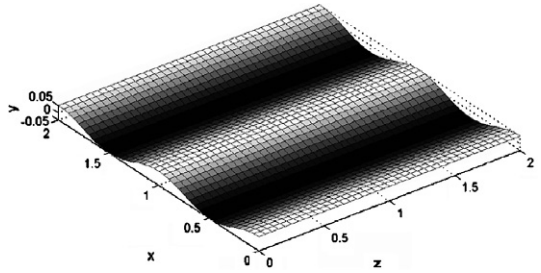

Fig. 1. Profile of the wavy wall characterized by $\alpha = 0.1$ and $\Lambda = 30$ mm.

$$y_w(x) = a\cos\left(\frac{2\pi x}{\Lambda}\right) \tag{1}$$

The mixed convective flow is characterized by the Reynolds number and the Grashof number. The Reynolds number Re_l is calculated according to

$$Re_l = \frac{U_B l}{\nu} \tag{2}$$

where ν denotes the kinematic viscosity, l represents the characteristic length scale, and the bulk velocity U_B is given by

$$U_B = \frac{1}{H - y_w}\int_{y_w}^{H} U(x_\xi, y)\mathrm{d}y \tag{3}$$

where x_ξ denotes an arbitrary x-location and y_w describes the profile of the complex surface. The Grashof number Gr_l is given by

$$Gr_l = \frac{g\Delta T\beta l^3}{\nu^2} \tag{4}$$

where ΔT denotes the temperature difference between the bottom and top wall, and β is the volumetric thermal expansion coefficient. The characteristic length scale l of the mixed convective channel flow can either be expressed as the distance between the thermally active walls, i.e. the channel height H, or it can be expressed in terms of the heating length x. The convective regime can be described by the ratio Gr_l/Re_l^2, which is unity for mixed convection, much smaller than one for forced convection, and much greater than one for natural convection when scaled with the channel height H (Incropera and DeWitt, 2002). Table 1 gives an overview over the experiments discussed in this paper. For reference purposes we investigated two isothermal flow conditions. The two non-isothermal flow conditions in the range of mixed convection are chosen in a way that for one natural convection is more dominant, for the other forced convection plays a larger role. The bulk velocities resemble laminar and turbulent flow regimes.

Table 1
Investigated flow conditions

Bulk velocity U_B(m/s)	Reynolds number		Grashof number		Ratio	
	Re_H	Re_x	Gr_H	Gr_x	Gr_H/Re_H^2	Gr_x/Re_x^2
0.031	1025	5.13×10^4	0	0	0	0
0.033	1100	5.50×10^4	1.94×10^6	2.43×10^{11}	1.60	80.16
0.064	2120	1.06×10^5	0	0	0	0
0.064	2120	1.06×10^5	1.30×10^6	1.63×10^{11}	0.28	14.16

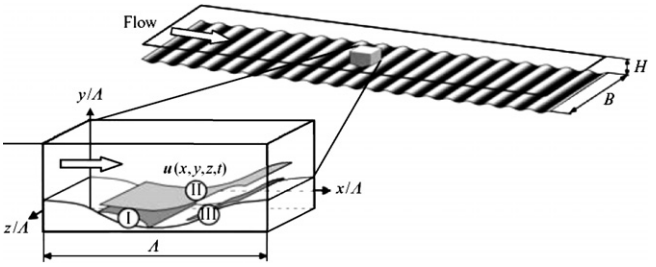

Fig. 2. Schematic of (I) the separation region, and the regions (II) of maximum positive and (III) maximum negative Reynolds shear stress for a flow situation with separation.

The flow over a train of solid waves is connected to a developing shear layer, formed by the separation of the flow shortly after the wave crest, which extends over the whole wavelength. Fig. 2 schematically illustrates characteristic regions of the flow field in the vicinity of the wavy surface reported by Cherukat et al. (1998), and Henn and Sykes (1999). These characteristic regions are the separation region (I), and the regions of maximum positive (II) and maximum negative (III) Reynolds shear stress $-\varrho\overline{u'v'}$. Füor smooth walls flow-oriented vortical eddies have been associated with large Reynolds stresses and with the production of turbulence in the viscous region close to the wall (Brooke and Hanratty, 1993). Günther and Rudolf von Rohr (2003), Kruse et al. (2003, 2006) and Kuhn et al. (2007) investigated the structure and dynamics of turbulent motions in a developed turbulent flow over complex surfaces and identified flow-oriented large-scale structures which contribute most to the momentum transport.

3. Experiments

The measurements are carried out in the channel facility depicted in Fig. 3. The working fluid is deionized and filtered water, the channel facility is made of anodized aluminium, PVC, and Schott BK-7 glass. All parts are positioned in a welded stainless steel frame. For a detailed description we refer to Günther and Rudolf von Rohr (2003). The full height of the channel, H, is 30 mm, and its aspect ratio (width B to height H) is 12:1. The wavy bottom wall in the test section is made of alumina and is heated with an embedded electrical heat foil ($\dot{q} = 1800$ W/m^2). Two temperature sensors are integrated in the top and bottom wall to record the temperature during the measurements at the measurement location. A heat exchanger is incorporated in the reservoir (9) to remove the heat from the fluid after passing the test section. Measurements confirmed a constant entry temperature of the fluid in the test section. Optical access is provided at four streamwise positions through viewing ports, positioned at both sidewalls and at the flat top wall. The measurements

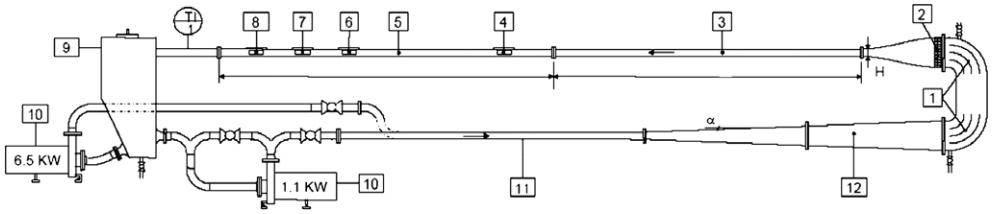

Fig. 3. Channel flow facility consisting of (1) turning elbows, (2) honeycomb, (3) flat-walled entrance section, (5) test section with complex bottom and flat top wall, (4, 6–8) optical viewports, (9) reservoir, (10) frequency controlled pumps, (11) pipe and (12) diffusor.

discussed in this paper are performed in the (x,y), and in the (x,z)-plane for a hydrodynamically developed flow after the 50th wave crest. Digital particle image velocimetry (DPIV) is performed to examine the spatial variation of the streamwise, vertical and spanwise velocity components (Adrian, 1991; Raffel et al., 1998; Westerweel, 1997). Planar laser-induced fluorescence (PLIF) is applied to study the structure of a dye plume which is emanated from a point source located at the wave crest in the measurement area (Karasso and Mungal, 1997; Shan et al., 2004). This point source consists of a canula with an inner diameter of 0.8 mm which is connected to a calibrated syringe pump, the inlet flow rate is adjusted to 0.25 ml/min. Both measurement techniques are combined to simultaneously assess the velocity and the scalar field. A flashlamp-pumped dual Nd:YAG-laser provides the pulse light source for both DPIV and PLIF. For DPIV the flow is seeded with hollow glass spheres with a mean diameter of 10 μm (density: 1.03 g/cm^3), the scattered light is recorded with a 10-bit CCD camera with a pixel-resolution of 1280×1024 pixels^2. As tracer for PLIF Rhodamine B in aqueous solution with an inlet concentration of 1×10^{-4} mol/l is used, the fluorescent light is recorded with a 12-bit CCD camera with a pixel-resolution of 1376×1040 pixels^2. To separate the Mie-scattering of the seeding particles from the fluorescent emission of the dye the DPIV camera is equipped with a band-pass filter (passing light at 532 nm $\pm$ 2 nm), the PLIF camera with a high-pass filter (cut-off below 540 nm). To perform simultaneous measurements the cameras, the laser and the image acquisition software were synchronized by means of an adjustable timing unit (PIV Synchronizer, ILA GmbH). We consider an ensemble of 1000 consecutive image pairs acquired at a frame rate of 4 Hz. The measurement system consisting of the laser, the laser optics, and the camera, is positioned on a traverse that allows vertical adjustment with an accuracy of approximately 10 μm. The post-processing of the DPIV data is comprised of an adaptive cross-correlation algorithm (Scarano and Riethmuller, 2000; Scarano, 2002), local filtering and interpolating of the filtered vectors. For PLIF a single pixel calibration is employed to account for inhomogeneities in the laser light sheet. In the post-processing the concentration information is then averaged over an area of 4×4 pixels^2 and is then mapped onto the velocity field.

4. Results

4.1. Velocity field

The field of view (FOV) of the measurements in the (x,y)-plane covers the whole region between the complex surface and the flat top wall (FOV $1.45H$ (streamwise) $\times$

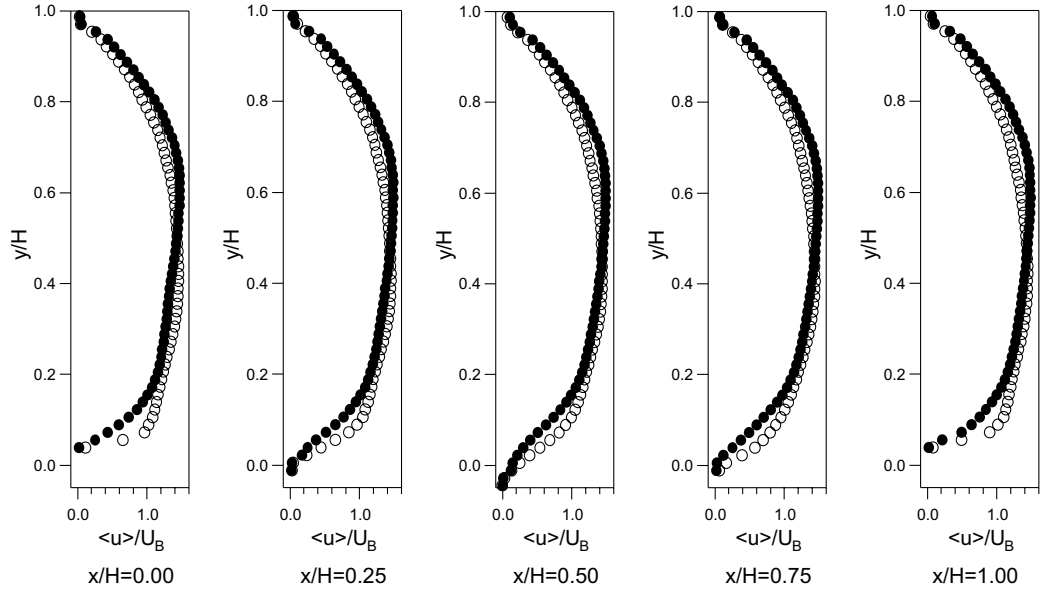

Fig. 4. Profiles of the mean velocity $\langle u \rangle / U_B$ along one wavelength for Reynolds numbers of $Re_H = 1025$ (unheated ●) and $Re_H = 1100$ (heated ○).

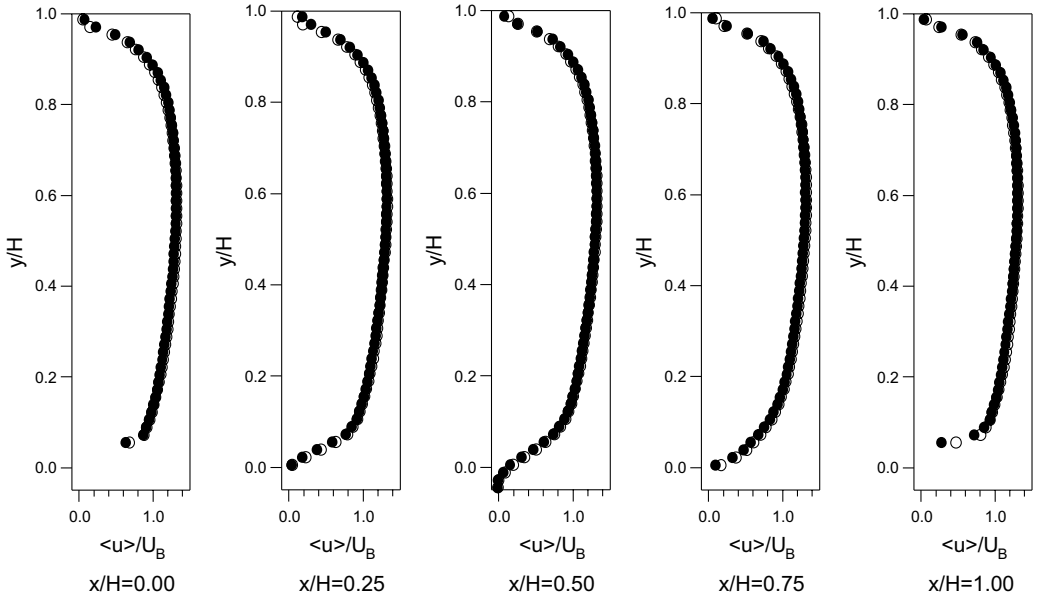

Fig. 5. Profiles of the mean velocity $\langle u\rangle/U_B$ along one wavelength for a Reynolds number of $Re_H = 2120$ (unheated ●, heated ○).

1.12H (vertical)). The spatial resolution of the PIV data in this plane of measurement is 0.016H, which corresponds to 480 μm. To characterize the influence of the heated bottom surface on the velocity field we plot profiles of turbulence quantities at constant streamwise positions along one wavelength, where $x/H = 0.00$ and $x/H = 1.00$ denotes the wave crest, $x/H = 0.50$ the wave trough.

4.1.1. Mean velocity profiles

Fig. 4 depicts the profiles of the normalized mean velocity $\langle u\rangle/U_B$ for a Reynolds number of $Re_H = 1025$ (unheated ●) and $Re_H = 1100$ (heated ○). In the unheated case the mean velocity profile is asymmetric. The location of maximum flow velocity is shifted towards the flat top wall and is found at a vertical coordinate of $y/H = 0.65$. This is consistent with earlier studies of isothermal flows over wavy walls at higher Reynolds numbers (e.g. Kruse et al., 2006). In the heated case also an asymmetric velocity profile is observed, however the location of maximum flow velocity is shifted towards the heated bottom surface ($y/H = 0.4$). In the complete region of the flow near the heated surface ($y/H < 0.2$) a higher mean streamwise velocity compared to the unheated case is observed. Negative values of the mean velocity in the region of the wave trough ($x/H = 0.50$) in

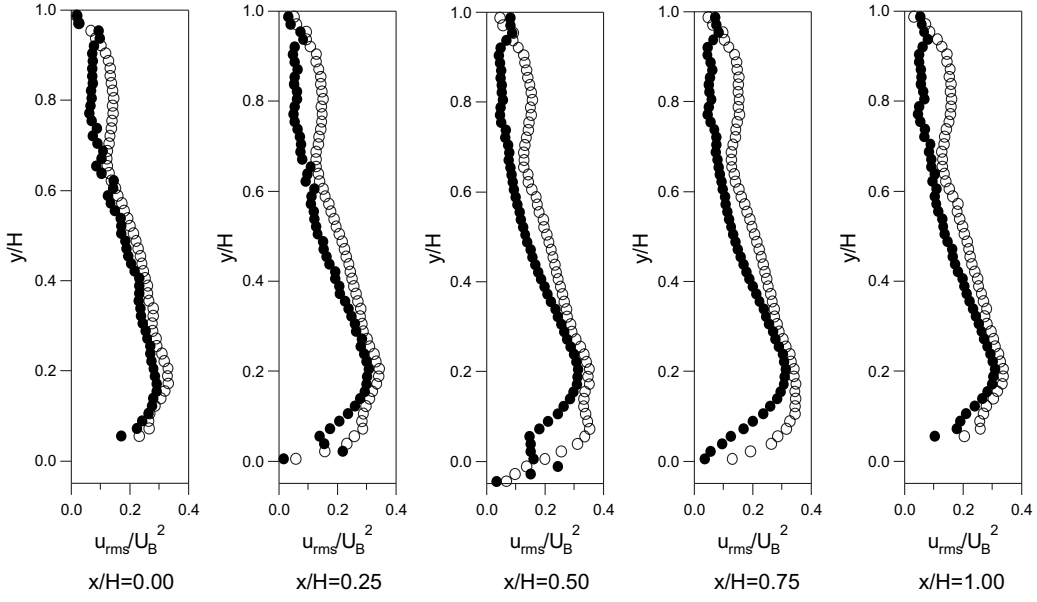

Fig. 6. Profiles of the root mean square of the streamwise velocity fluctuation $\sqrt{\langle u'^2\rangle}/U_B$ along one wavelength for Reynolds numbers of $Re_H = 1025$ (unheated ●) and $Re_H = 1100$ (heated ○).

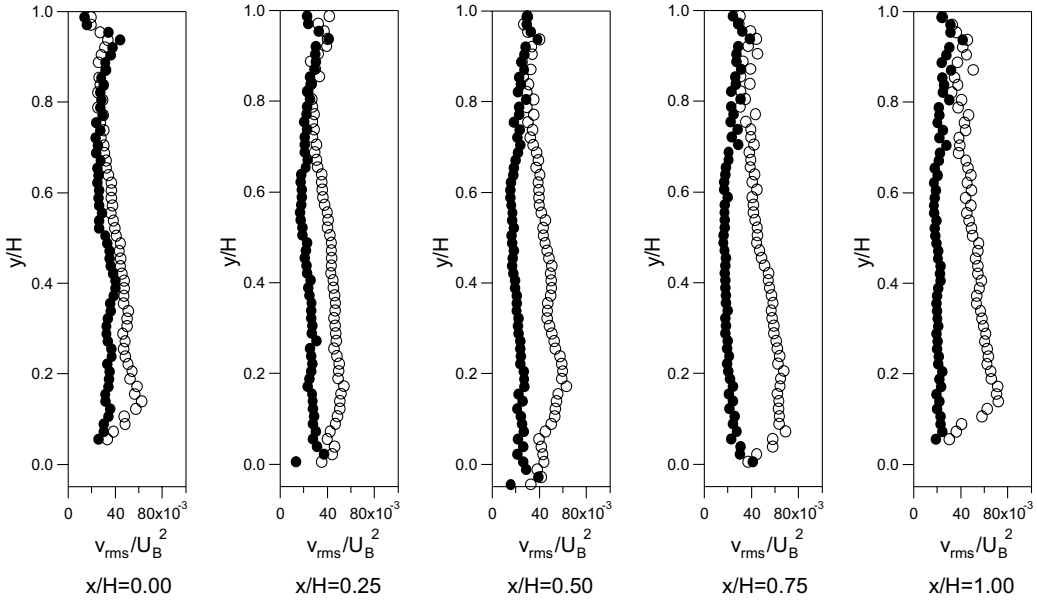

Fig. 7. Profiles of the root mean square of the vertical velocity fluctuation $\sqrt{\langle v'^2\rangle}/U_B$ along one wavelength for Reynolds numbers of $Re_H = 1025$ (unheated ●) and $Re_H = 1100$ (heated ○).

the heated case indicate a separated flow region. This is not found in the isothermal case. Fig. 5 compares the mean velocity profiles for the unheated (●) and heated (○) case for the Reynolds number $Re_H = 2120$. For this flow condition the ratio Gr_H/Re_H^2 equals 0.28, which means that the influence of forced convection is increased. This becomes apparent in the mean velocity profiles which overlap for both cases. The location of maximum flow velocity is found at a vertical coordinate of $y/H = 0.6$, negative mean velocity values at the streamwise position $x/H = 0.50$ indicate flow separation. The only differences in the mean valued are found in the region close to the wall ($y/H < 0.1$). In this near wall region the mean velocity is slightly increased compared to the isothermal case.

4.1.2. Root mean square of velocity fluctuations

To further characterize the influence of the heated wavy surface we calculate the normalized root mean squares of the velocity fluctuations $\sqrt{\langle u'^2\rangle}/U_B$, respectively $\sqrt{\langle v'^2\rangle}/U_B$. Fig. 6 depicts the profiles of the root mean square of the streamwise velocity fluctuation along one wavelength for the Reynolds number $Re_H = 1025$ (unheated ●) and

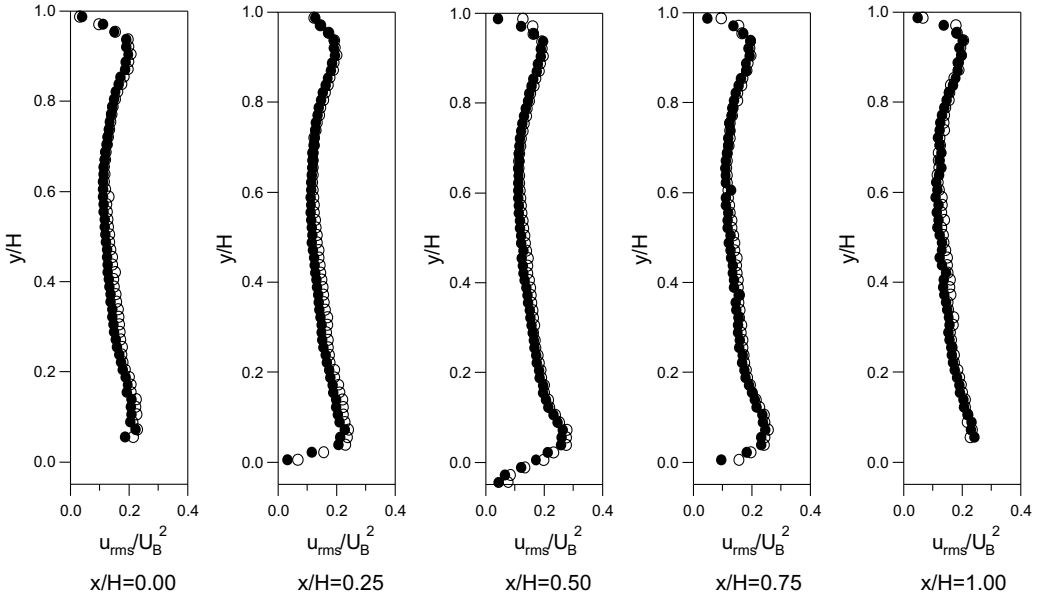

Fig. 8. Profiles of the root mean square of the streamwise velocity fluctuation $\sqrt{\langle u'^2\rangle}/U_B$ along one wavelength for a Reynolds number of $Re_H = 2120$ (unheated ●, heated ○).

$Re_H = 1100$ (heated ○). For the heated case in general larger values of the root mean square are found, especially in the region near the heated wavy surface. At the location of the wave crest, i.e. $x/H = 0.00$ and $x/H = 1.00$, the profiles nearly overlap. Downstream and upstream of the wave crest and in the wave trough a maxima is found at a vertical position of approximately $y/H = 0.1$. This indicates that the fluid inside the wave trough accumulates more heat resulting in higher local fluid velocities compared to the isothermal case. A second maxima of the root mean square of the streamwise velocity fluctuations is located in the upper half of the channel near the flat top wall at $y/H \approx 0.8$. This could be an indication of large-scale thermal structures reported in an earlier study (Kruse and Rudolf von Rohr, 2006). Fig. 7 depicts the profiles of the root mean square of the vertical velocity fluctuations along one wavelength for the Reynolds number $Re_H = 1025$ (unheated ●) and $Re_H = 1100$ (heated ○). In the profiles the influence of buoyancy due to the resulting fluid motion in vertical direction is observed. In the region between the heated bottom surface and the dimensionless coordinate of $y/H = 0.8$ larger rms values of the vertical velocity fluctuations are found. These results allow to determine the region of the flow which is directly affected by mixed convection. Figs. 8 and 9 depict the pro-

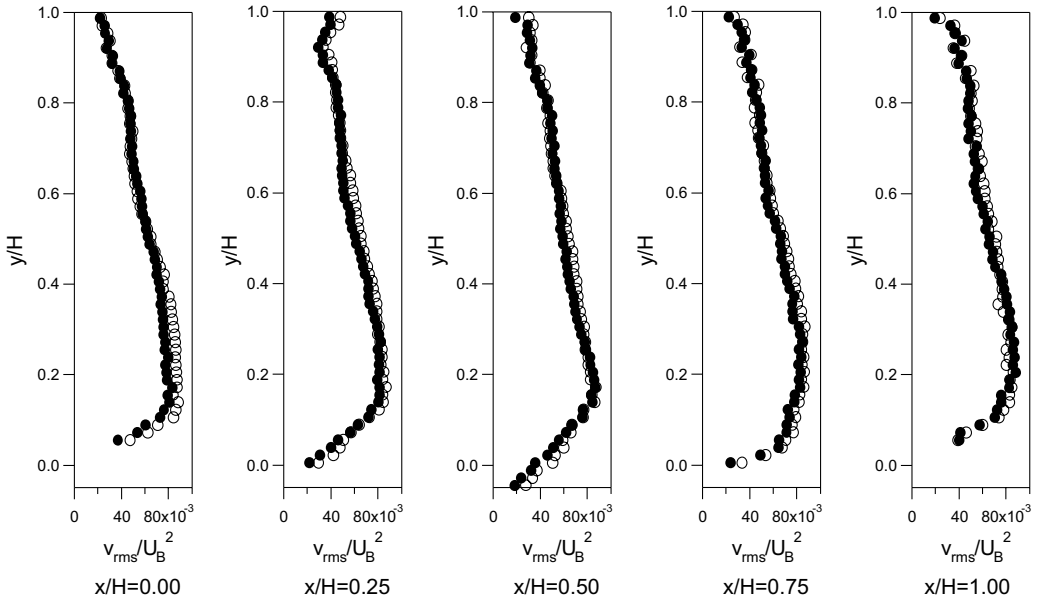

Fig. 9. Profiles of the root mean square of the vertical velocity fluctuation $\sqrt{\langle v'^2 \rangle}/U_B$ along one wavelength for a Reynolds number of $Re_H = 2120$ (unheated ●, heated ○).

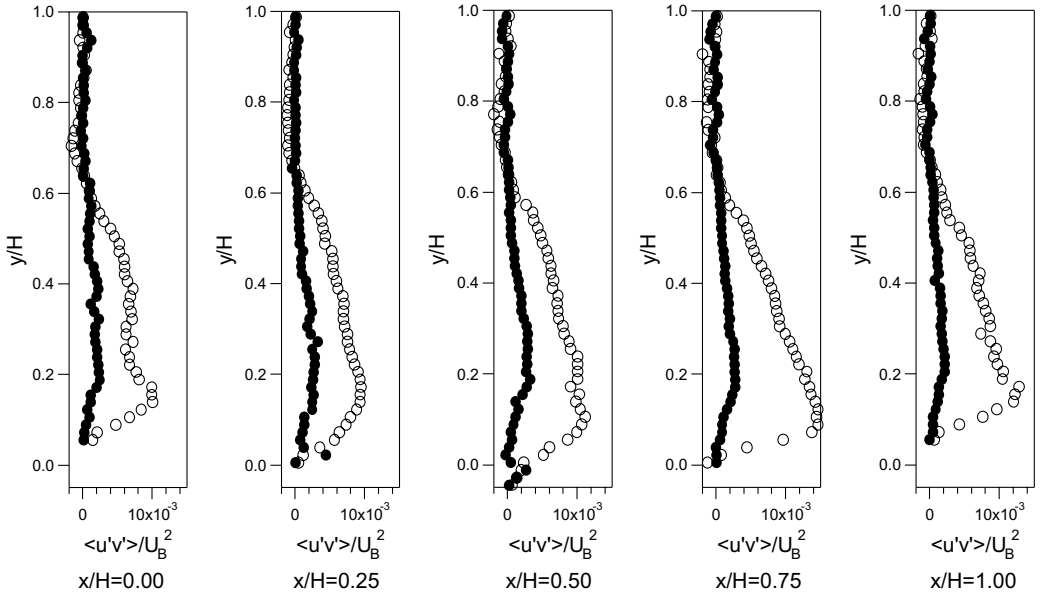

Fig. 10. Profiles of the Reynolds stress $\langle u'v' \rangle / U_B^2$ along one wavelength for Reynolds numbers of $Re_H = 1025$ (unheated ●) and $Re_H = 1100$ (heated ○).

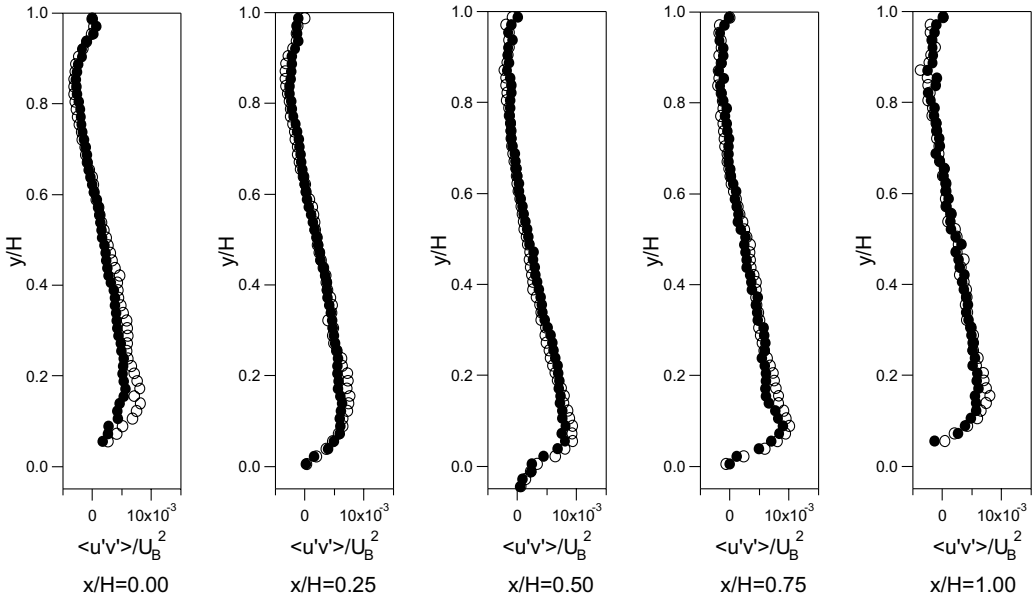

Fig. 11. Profiles of the Reynolds stress $\langle u'v' \rangle / U_B^2$ along one wavelength for a Reynolds number of $Re_H = 2120$ (unheated ●, heated ○).

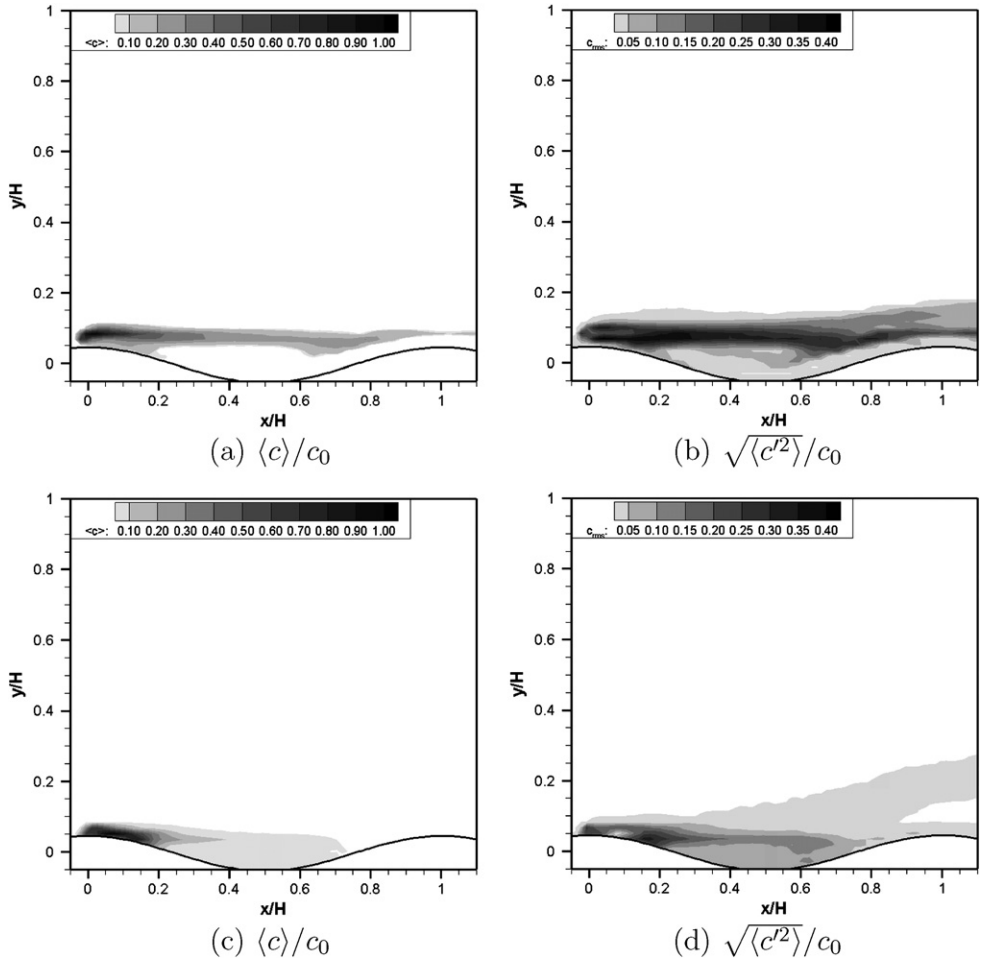

Fig. 12. Contours of the mean concentration field and the root mean square of the concentration fluctuations for a Reynolds number of $Re_H = 1025$ (unheated, first row) and of $Re_H = 1100$ (heated, second row). The point source is located at $x/H = 0.00$, $y/H = 0.05$.

files of the root mean square values of the velocity fluctuations for the unheated (●) and heated (○) case at the Reynolds number $Re_H = 2120$. The profiles nearly overlap, only small deviations due to the influence of mixed convection compared to the turbulent motion induced by the presence of the wavy surface are observed.

4.1.3. Reynolds stress

The flow over waves is associated with a shear layer developing after the wave crest and extending over the whole wavelength. For mixed convection this shear layer is expected to be intensified through the interaction between the mean flow and the upward fluid motion due to buoyancy. Fig. 10 depicts the profiles of the Reynolds stress along one wavelength for the Reynolds number $Re_H = 1025$ (unheated ●) and $Re_H = 1100$ (heated ○). Larger values of the Reynolds stress are found in the region between the heated wavy surface and the location $y/H = 0.6$. The location of the maxima changes from a vertical coordinate of $y/H = 0.15$ for the wave crests to $y/H = 0.10$ in the wave trough. At the upstream side of the wave crest ($x/H = 0.75$) a pronounced Reynolds stress profile is found. This indicates that the mixed convection is also influenced by the local curvature of the wall. Fig. 11 compares the Reynolds stress profiles for the unheated (●) and heated (○) case for the Reynolds number $Re_H = 2120$. For this flow situation the only differences in the Reynolds stresses are found in the region close to the wall ($y/H < 0.2$), where the Reynolds stresses are enlarged.

4.2. Scalar field

The LIF measurements in the (x, y)-plane are performed in the same field of field as the PIV measurements described in the last section (FOV $1.45H$ (streamwise) $\times$ $1.12H$ (vertical)). The spatial resolution of the LIF data is $0.008H$, which corresponds to 252 μm. The field of view for the measurements in the (x, z)-plane is $0.87H$ (streamwise) $\times$ $1.14H$ (spanwise), which corresponds to a spatial resolution of the LIF data of $0.0067H$, respectively 200 μm. For all measurements the point source is located at the wave crest, all values presented are made dimensionless with the source concentration c_0.

4.2.1. Mean concentration and concentration fluctuation field in the (x, y)-plane

Fig. 12 depicts contours of the mean concentration and the root mean square of the concentration fluctuations at Reynolds number $Re_H = 1025$ (unheated, first row), respectively $Re_H = 1100$ (heated, second row). Both, in the mean and the fluctuating concentration field the influence of mixed convection is visible. In the unheated case

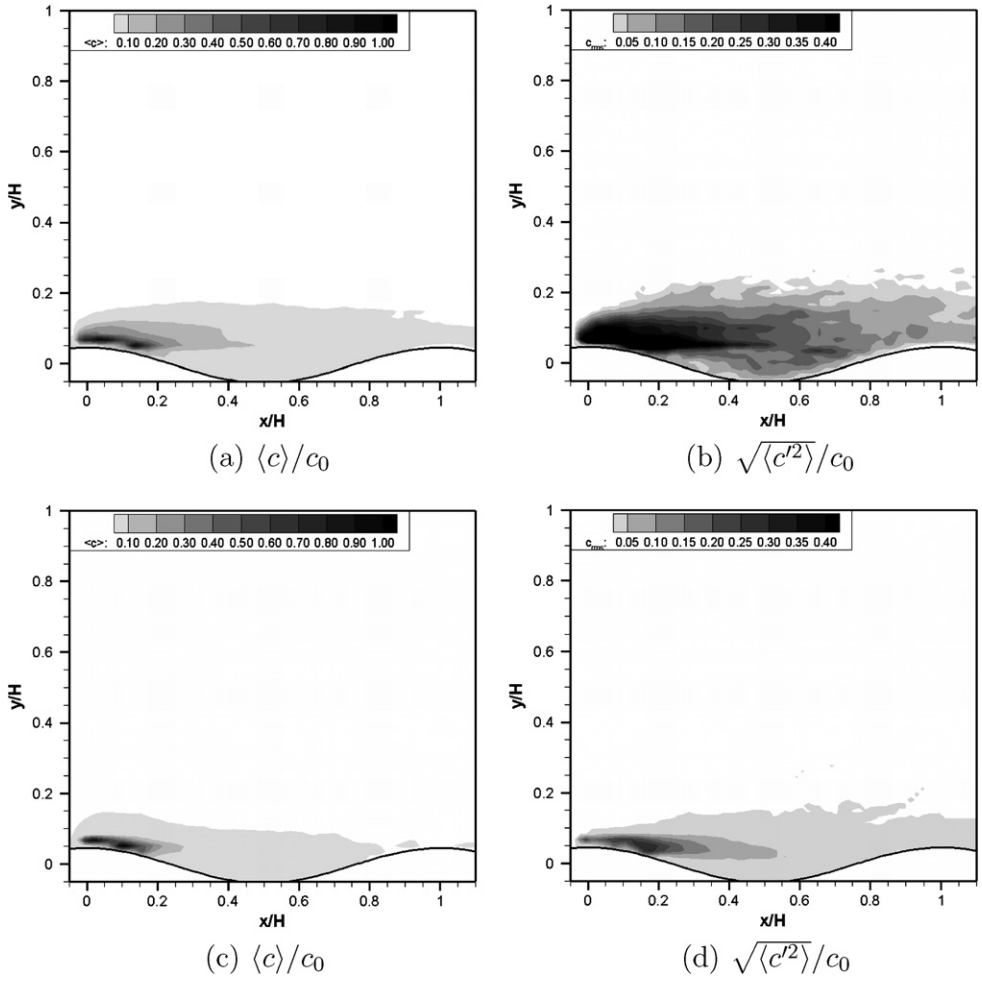

Fig. 13. Contours of the mean concentration field and the root mean square of the concentration fluctuations for a Reynolds number of $Re_H = 2120$ for the unheated case (first row) and the heated case (second row). The point source is located at $x/H = 0.00$, $y/H = 0.05$.

the scalar is convected with the mean flow, no transport in vertical direction is observed. This is confirmed by the root mean square values of the concentration fluctuations where also no indication of vertical transport is found. The rather small rms values in the wave trough could result from instantaneous flow separation and the instantaneous formation of a recirculation zone, both not pronounced in the mean flow field. For the heated case the dilution of the mean scalar field along one wavelength is observed. This is an indication of longitudinal flow structures induced by the mixed convection from the heated surface which increase the spanwise transport. The contours of the mean concentration field depict also some amount of the tracer dye being transported into the wave trough. This is an indication of flow separation and the presence of a recirculation zone in the mean flow field. The root mean square values exhibit increased vertical transport at the upstream side of the wave. We will characterize the dominant scalar structures of this vertical transport in the next section. Fig. 13 depicts contours of the mean concentration and the root mean square of the concentration fluctuations at a Reynolds number of $Re_H = 2120$ for the unheated case (first row) and the heated case (second row). For the unheated case the transport of the scalar with the mean flow is observed, the root mean square values show some transport in vertical direction which is due to the presence of the wavy surface. In the heated case the dilution of the mean concentration field along one wavelength is found as well as the vertical transport of the tracer dye. Compared to the mixed convective flow at a Reynolds number of $Re_H = 1100$ the transport in vertical direction is decreased but still more pronounced than in both unheated cases.

To identify the dominant scalar structures with the largest impact on the vertical transport we investigate instantaneous realizations of the scalar concentration field. Fig. 14 depicts such instantaneous realizations for $Re_H = 1100$ and $Gr_H = 1.94 \times 10^6$, respectively $Gr_x = 2.43 \times 10^{11}$ (Fig. 14(a) and (b)), and as a reference for $Re_H = 1025$ and $Gr_H = Gr_x = 0$ (Fig. 14(c)). Fig. 14(a) depicts a typical ejection of the tracer dye into the outer flow which is also found for mixed convective flows over flat surfaces. Due to buoyancy differences the scalar moves along with packets of rising fluid and is thus transported in vertical

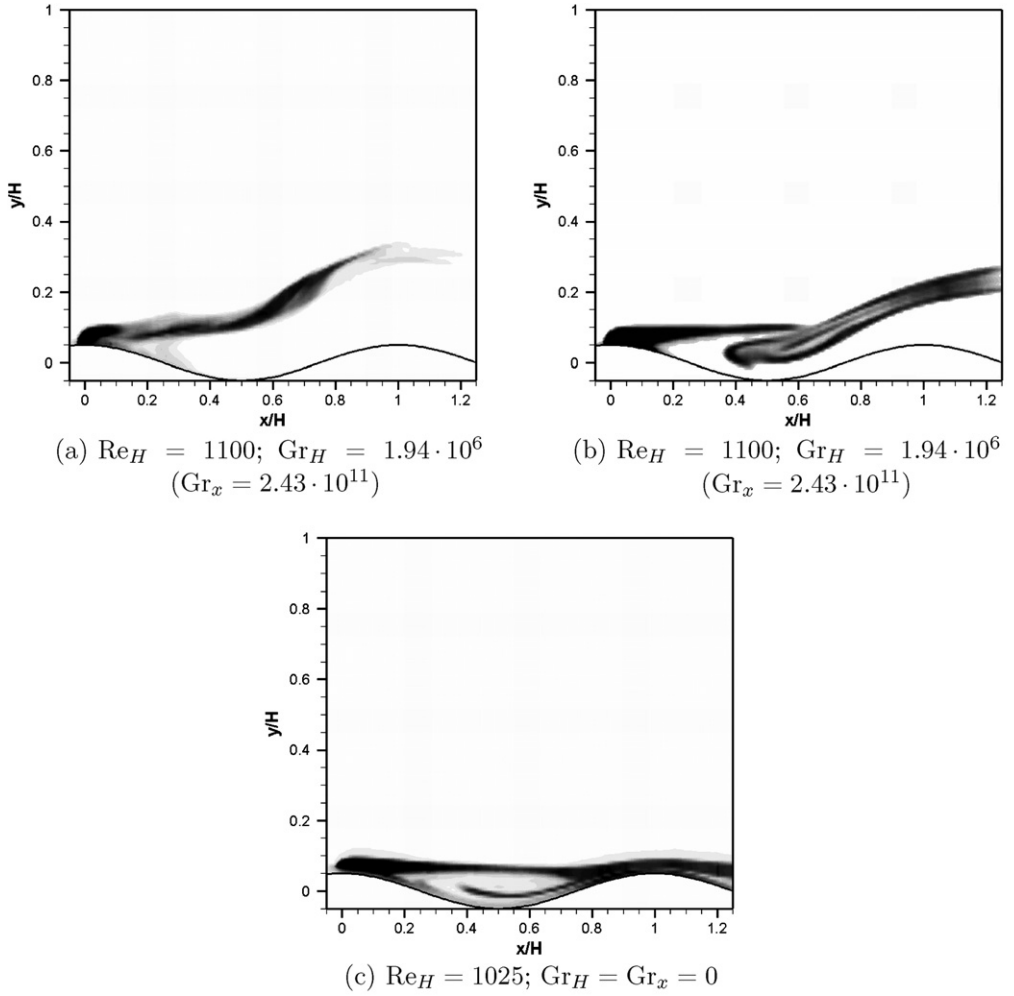

(a) $\mathrm{Re}_H = 1100;\ \mathrm{Gr}_H = 1.94 \cdot 10^6$ $(\mathrm{Gr}_x = 2.43 \cdot 10^{11})$

(b) $\mathrm{Re}_H = 1100;\ \mathrm{Gr}_H = 1.94 \cdot 10^6$ $(\mathrm{Gr}_x = 2.43 \cdot 10^{11})$

(c) $\mathrm{Re}_H = 1025;\ \mathrm{Gr}_H = \mathrm{Gr}_x = 0$

Fig. 14. Instantaneous realizations of the scalar concentration field. The point source is located at $x/H = 0.00$, $y/H = 0.05$.

direction. Fig. 14(b) depicts the second prevailing scalar structure. The tracer dye is first trapped in the wave trough and then ejected into the outer flow at the upstream side of the wave. Thus this vertical transport is based on the combination of buoyancy effects and the effects induced by the local wall curvature. An analysis of the image ensemble yields a dominance of the latter described mechanism. Thus we conclude an additional enhancement of transport properties due to the presence of the wavy surface.

4.2.2. Mean concentration and concentration fluctuation field in the (x, z)-plane

To address the effects of longitudinal flow structures present in the flow field we investigate the spanwise spreading of the scalar plume in the (x, z)-plane. The laser light sheet is adjusted to a plane 1 mm above the wavy surface. Fig. 15 depicts contours of the mean concentration and the root mean square of the concentration fluctuations at Reynolds number $Re_H = 1025$ (unheated, first row), respectively $Re_H = 1100$ (heated, second row). For the unheated case no spanwise transport of the scalar in the mean concentration field is observed. The undulation in the region $0.2 \leqslant x/H \leqslant 0.6$ originates from tracer dye which is accumulating in the wave trough and is not due to transport processes. This is consistent with the rms concentration field, where also only a small spanwise spreading is found. In the case of mixed convection a meandering of the scalar plume induced by longitudinal flow structures is observed. This leads to the spanwise spreading of the mean scalar field, and is especially pronounced when calculating the rms concentration field. Thus the spanwise scalar transport is greatly enhanced by mixed convection compared to the isothermal case. Fig. 16 depicts contours of the mean concentration and the root mean square of the concentration fluctuations at a Reynolds number of $Re_H = 2120$ for the unheated case (first row) and the heated case (second row). For this Reynolds number the flow is in the transition

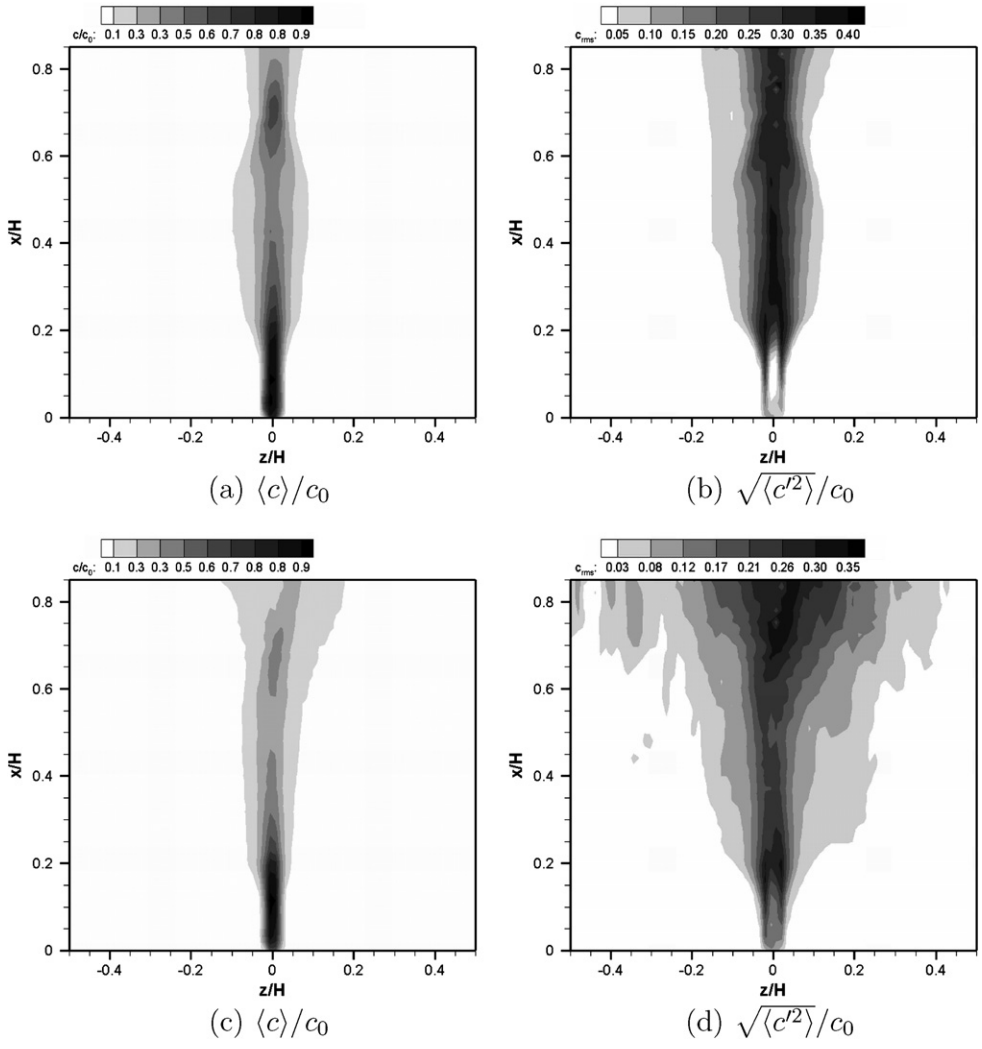

Fig. 15. Contours of the mean concentration field and the root mean square of the concentration fluctuations for a Reynolds number of $Re_H = 1025$ (unheated, first row) and of $Re_H = 1100$ (heated, second row). The point source is located at $x/H = 0.00$, $z/H = 0.00$.

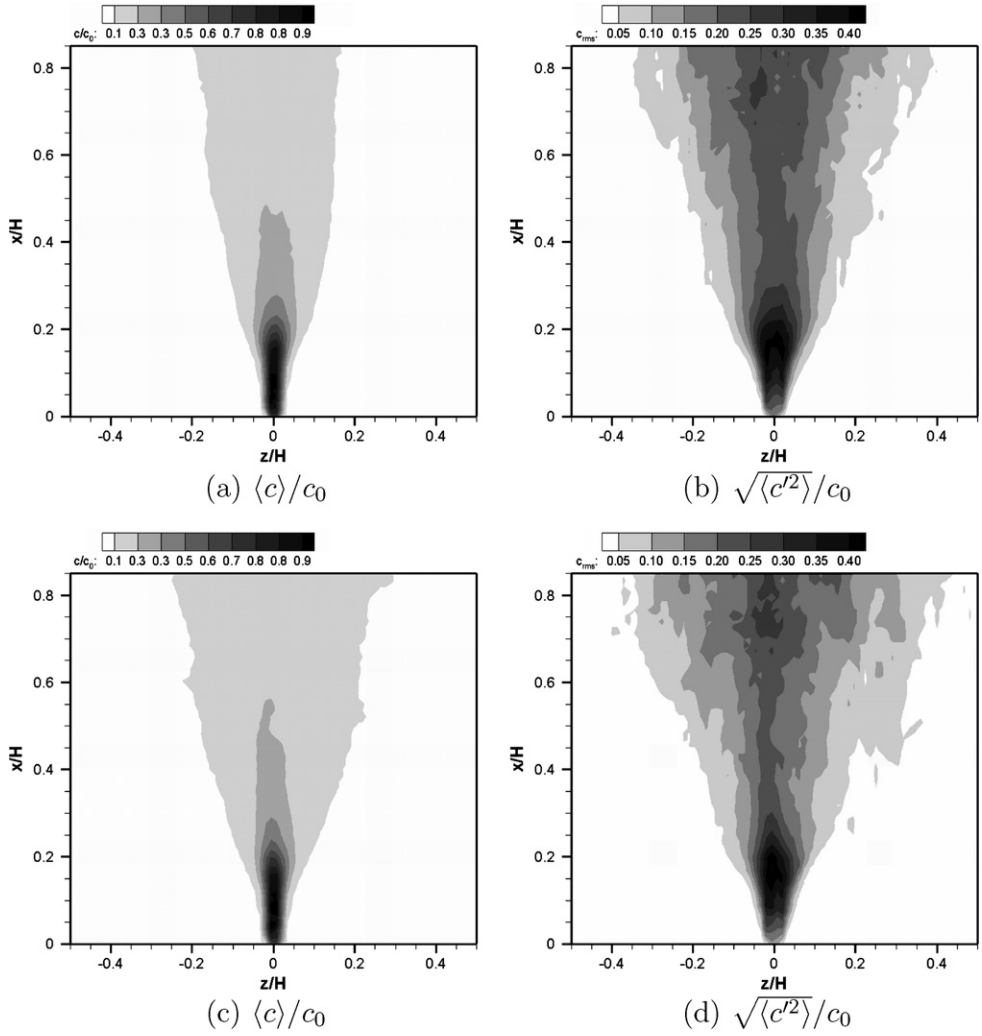

Fig. 16. Contours of the mean concentration field and the root mean square of the concentration fluctuations for a Reynolds number of $Re_H = 2120$ for the unheated case (first row) and the heated case (second row). The point source is located at $x/H = 0.00$, $z/H = 0.00$.

to turbulence, thus also for the unheated case a spanwise transport is observed for both the mean and the rms concentration field. However, this spanwise transport is additionally enhanced by mixed convection. It is worth noting that the rms intensities in both heated cases at $Re_H = 1100$ and $Re_H = 2120$ are comparable. Thus we obtain comparable spanwise transport due to mixed convection which is independent of the flow regime, i.e. if the flow is nominally laminar or turbulent.

5. Conclusions

We apply a combined DPIV/PLIF technique to address mixed convection from a wavy surface and the additional transport of a scalar (injected tracer dye). The flow between the flat top and heated wavy bottom surface is investigated at two different Reynolds numbers, in each case heated and isothermal. By recording long image series the statistics of the velocity and the concentration field are calculated and we discuss the influence of mixed convection on turbulence quantities and scalar transport properties.

We identified a shift of the mean velocity profile in the vicinity of the heated surface and a separation zone downstream of the wave, both effects not present in the isothermal case. By calculating the root mean square values of the velocity fluctuations and the Reynolds stress we concluded that momentum transport is increased for the mixed convection regime. The transport of the tracer dye is characterized by enhanced vertical transport due to buoyancy effects and enhanced spanwise transport due to the presence of longitudinal flow structures induced by the mixed convection. This spanwise transport in mixed convection is comparable for laminar and turbulent flow conditions.

By analyzing instantaneous realizations of the scalar concentration field we identify two dominant scalar structures contributing most to vertical transport. The first one is characterized by the vertical transport of the tracer dye with rising packets of fluid with decreased density, i.e. induced by buoyancy effects. The second one results from a combination of buoyancy effects and local wall curvature, the tracer dye is trapped in the wave trough and is then transported in the outer flow at the upstream side of

the wave. The latter described transport mechanism occurs at a higher frequency compared to the first. Thus the transport properties are additionally enhanced compared to mixed convection from a flat plate by the presence of the wavy surface.

Acknowledgements

We gratefully acknowledge financial support from the Swiss National Science Foundation (SNF). Measurement technology is partially provided by ILA GmbH.

References

Adrian, R.J., 1991. Particle-imaging techniques for experimental fluid mechanics. Annu. Rev. Fluid Mech. 23, 261–304.

Angirasa, D., Peterson, G.P., Pop, I., 1997. Combined heat and mass transfer by natural convection with opposing bouyancy effects in a fluid saturated porous medium. Int. J. Heat Mass Transf. 40 (12), 2755–2773.

Ayinde, T.F., Said, S.A.M., Habib, M.A., 2006. Experimental investigation of turbulent natural convection flow in a channel. Heat Mass Transf. 42 (3), 169–177.

Banna, M., Pietri, L., Zeghmati, B., 2004. Turbulent mixed convection of heat and water vapor transfers in a two-dimensional vegetation canopy. Heat Mass Transf. 40, 757–768.

Brooke, J.W., Hanratty, T.J., 1993. Origin of turbulence-producing eddies in a channel flow. Phys. Fluids A5 (4), 1011–1022.

Cherukat, P., Na, Y., Hanratty, T.J., McLaughlin, J.B., 1998. Direct numerical simulation of a fully developed turbulent flow over a wavy wall. Theoret. Comp. Fluid Dynam. 11, 109–134.

Dellil, A.Z., Azzi, A., Jubran, B.A., 2004. Turbulent flow and convective heat transfer in a wavy wall channel. Heat Mass Transf. 40, 793–799.

Evans, G., Greif, R., Siebers, D., Tieszen, S., 2005. Turbulent mixed convection from a large, high temperature, vertical flat surface. Int. J. Heat Fluid Flow 26, 1–11.

Günther, A., Rudolf von Rohr, P., 2003. Large-scale structures in a developed flow over a wavy wall. J. Fluid Mech. 478, 257–285.

Henn, D.S., Sykes, R.I., 1999. Large-eddy simulation of flow over wavy surfaces. J. Fluid Mech. 383, 75–112.

Incropera, F.P., DeWitt, D.P., 2002. Fundamentals of heat and mass transfer. John Wiley & Sons.

Jang, J.-H., Yan, W.-M., 2004. Mixed convection heat and mass transfer along a vertical wavy surface. Int. J. Heat Mass Transf. 47, 419–428.

Karasso, P.S., Mungal, M.G., 1997. PLIF measurements in aqueous flows using the Nd:YAG laser. Exp. Fluids 23, 382–387.

Krettenauer, K., Schumann, U., 1989. Direct numerical simulation of thermal convection over a wavy surface. Meteorol. Atmos. Phys. 41, 165–179.

Kruse, N., Rudolf von Rohr, P., 2006. Structure of turbulent heat flux in a flow over a heated wavy wall. Int. J. Heat Mass Transf. 49 (19-20), 3514–3529.

Kruse, N., Günther, A., Rudolf von Rohr, P., 2003. Dynamics of large-scale structures in turbulent flow over a wavy wall. J. Fluid Mech. 485, 87–96.

Kruse, N., Kuhn, S., Rudolf von Rohr, P., 2006. Wavy wall effects on turbulence production and large-scale modes. J. Turbulence 7 (31), 1–24.

Kuhn, S., Wagner, C., Rudolf von Rohr, P., 2007. Influence of wavy surfaces on coherent structures in a turbulent flow. Exp. Fluids 43, 251–259.

Lin, M.H., Chen, C.T., 2006. Effect of rotation on the formation of longitudinal vortices in mixed convection flow over a flat plate. Heat Mass Transf. 42 (3), 178–186.

Maughan, J.R., Incropera, F.P., 1989. Regions of heat transfer enhancement for laminar mixed convection in a parallel plate channel. Int. J. Heat Mass Transf. 33, 555–570.

Metwally, H.M., Manglik, R.M., 2004. Enhanced heat transfer due to curvature-induced lateral vortices in laminar flows in sinusoidal corrugated-plate channels. Int. J. Heat Mass Transf. 47, 2283–2292.

Moulic, S.G., Yao, L.S., 1989. Mixed convection along a wavy surface. J. Heat Transf. 111, 974–979.

Osborne, D.G., Incropera, F.P., 1985a. Laminar, mixed convection heat transfer for flow between horizontal plates with asymmetric heating. Int. J. Heat Mass Transf. 28, 207–217.

Osborne, D.G., Incropera, F.P., 1985b. Experimental study of mixed convection heat transfer for transitional and turbulent flow between horizontal, parallel plates. Int. J. Heat Mass Transf. 28 (7), 1337–1344.

Raffel, M., Willert, C., Kompenhans, J., 1998. Particle Image Velocimetry. A practical guide. Springer.

Rush, T.A., Newell, T.A., Jacobi, A.M., 1999. An experimental study of flow and heat transfer in sinusoidal wavy passages. Int. J. Heat Mass Transf. 42, 1541–1553.

Scarano, F., 2002. Iterative image deformation methods in PIV. Meas. Sci. Technol. 13, R1–R19.

Scarano, F., Riethmuller, M.L., 2000. Advances in iterative multigrid PIV image processing. Exp. Fluids 29, S51–S60.

Shan, J.W., Lang, D.B., Dimotakis, P.E., 2004. Scalar concentration measurements in liquid-phase flows with pulsed lasers. Exp. Fluids 36, 268–273.

Westerweel, J., 1997. Fundamentals of digital particle image velocimetry. Meas. Sci. Technol. 8, 1379–1392.

Yao, L.S., 1983. Natural convection along a vertical wavy surface. J. Heat Transf. 105, 465–468.

Yu, C.H., Chang, M.Y., Lin, T.F., 1997a. Structures of moving transverse and mixed rolls in mixed convection of air in a horizontal plane channel. Int. J. Heat Mass Transf. 40 (2), 333–346.

Yu, C.H., Chang, M.Y., Huang, C.C., Lin, T.F., 1997b. Unsteady vortex roll structures in a mixed convective air flow through a horizontal plane channel: a numerical study. Int. J. Heat Mass Transf. 40 (3), 505–518.

Zhang, H., Huang, X.Y., Li, H.S., Chua, L.P., 2002. Flow patterns and heat transfer enhancement in low-Reynolds–Rayleigh-number channel flow. Appl. Therm. Eng. 22, 1277–1288.